other than the methyltransferase, resulting in hypermethylation of some genomic regions. If this hypothesized component were mutated in the *clk* lines, this might cause only a portion of the AMT phenotype, namely, hypermethylation of *SUP*.

Note added in proof: We have found a *clk*-like pattern of methylation at the SUP locus in fonl-2 and fonl-3 [see (*14*)].

REFERENCES AND NOTES

1. R. A. Martienssen and E. J. Richards, *Curr. Opin. Genet. Dev.* **5**, 234 (1995).
2. A. Vongs, T. Kakutani, R. A. Martienssen, E. J. Richards, *Science* **260**, 1926 (1993); T. Kakutani, J. A. Jeddeloh, S. K. Flowers, K. Munakata, E. J. Richards, *Proc. Natl. Acad. Sci. U.S.A.* **93**, 12406 (1996).
3. E. J. Finnegan, W. J. Peacock, E. S. Dennis, *Proc. Natl. Acad. Sci. U.S.A.* **93**, 8449 (1996).
4. M. J. Ronemus, M. Galbiati, C. Ticknor, J. Chen, S. L. Dellaporta, *Science* **273**, 654 (1996).
5. *clk-2* and *clk-3* were from an ethylmethanesulfonate mutagenesis, *clk-5* from a diepoxybutane mutagenesis, and *clk-6* from a transferred-DNA insertional mutagenesis. *clk-1*, *clk-4*, and *clk-7* were from the *fwa-1*, *gl2-1*, and *tt2-1* mutants, respectively, obtained from the Arabidopsis Biological Resource Center. All alleles are in the Ler background.
6. J. L. Bowman *et al.*, *Development* **114**, 599 (1992); E. A. Schultz, F. B. Pickett, G. W. Haughn, *Plant Cell* **3**, 1221 (1991).
7. J. C. Gaiser, K. Robinson-Beers, C. S. Gasser, *Plant Cell* **7**, 333 (1995).
8. H. Sakai and E. M. Meyerowitz, personal communication.
9. Wild-type plants usually have two carpels per flower, but occasionally have extra carpels. *clk* and *sup* heterozygotes contain more extra carpels than the wild type. Whereas Ler plants had 0.2 ± 0.2 extra carpels per plant (mean ± SE) in the first 10 flowers, *clk-3* heterozygotes had 3.3 ± 0.7, and *sup-5* heterozygotes had 2.1 ± 0.7.
10. C. Chang, J. L. Bowman, A. W. DeJohn, E. Lander, E. M. Meyerowitz, *Proc. Natl. Acad. Sci. U.S.A.* **85**, 6856 (1988).
11. H. Sakai, L. J. Medrano, E. M. Meyerowitz, *Nature* **378**, 199 (1995).
12. Genomic DNA from Ler or *clk-3* plants was partially digested with Sau 3A and cloned in the LambdaGEM-11 vector (Promega). The adjacent 5.5- and 1.2-kb Eco RI *SUP* genomic fragments (*11*) were subcloned from hybridization-selected lambda clones into the plant transformation vector pCGN1547 [K. E. McBride and K. R. Summerfelt, *Plant Mol. Biol.* **14**, 269 (1990)] and then transformed into either *clk-3* or *sup-5* plants [N. Bechtold, J. Ellis, G. Pelletier, *C. R. Acad. Sci. Paris* **316**, 1194 (1993)].
13. CosTH1 was isolated from a Wassilewskija genomic cosmid library (Arabidopsis Biological Resource Center) and contains a 25-kb insert that partially overlaps the proximal side of the *SUP* 6.7-kb genomic region. An overlapping set of cosmid clones on the distal side of *SUP* (LM5-2, LM5-8, Q8PMI, Pst14.5, Pst11, and Bam5.5) was a gift from H. Sakai.
14. Recently, three mutants were described [H. Huang and H. Ma, *Plant Cell* **9**, 115 (1997)] that also have a weak *sup*-like phenotype. Although the authors interpreted these mutations as being in a previously unidentified gene near *SUP*, it seems possible that these are also epigenetic *SUP* alleles.
15. M. Koornneef, S. W. M. Dellaert, J. H. van der Veen, *Mutat. Res.* **93**, 109 (1982).
16. S. E. Jacobsen and E. M. Meyerowitz, data not shown.
17. Genomic DNA from whole shoots was used for bisulfite sequencing [R. Feil, J. Charlton, A. P. Bird, J. Walter, W. Reik, *Nucleic Acids Res.* **22**, 695 (1994)]. Seven overlapping polymerase chain reaction (PCR) amplifications were used to determine the methylation pattern shown in Fig. 3. PCR products were sequenced with Amplitaq DNA Polymerase FS dye terminator cycle sequencing (Perkin-Elmer).
18. The *SUP* cDNA was used to probe genomic DNA blots at various stringencies. Under high-stringency conditions (*10*), only the *SUP* gene is detected. At lower washing stringency (2× saline sodium phosphate EDTA, 0.5% SDS, 55°C), an additional band is detected. This hybridizing fragment was cloned and found to contain a region of homology limited to a 101-bp sequence, encoding a zinc-finger domain, which shares 76% nucleic acid identity with *SUP*.
19. D. R. Smyth, J. L. Bowman, E. M. Meyerowitz, *Plant Cell* **2**, 755 (1990).

20. We thank G. Serraiocco for technical assistance, H. Sakai for *SUP* genomic sequences and cosmid clones, E. Finnegan and E. Dennis for the AMT line, D. Weigel for *clk-5*, J. Viret and E. Signer for *clk-6*, and X. Chen, J. Fletcher, M. Frohlich, J. Hua, C. Ohno, J. L. Riechmann, R. Sablowski, H. Sakai, D. Wagner, and E. Ziegelhoffer for review of the manuscript. S.E.J. was supported by an NIH postdoctoral fellowship. This work was supported by NSF grant MCB-9204839 to E.M.M.

10 April 1997; accepted 11 July 1997

In Situ Activation Pattern of *Drosophila* EGF Receptor Pathway During Development

Limor Gabay, Rony Seger, Ben-Zion Shilo*

Signaling cascades triggered by receptor tyrosine kinases (RTKs) participate in diverse developmental processes. The active state of these signaling pathways was monitored by examination of the in situ distribution of the active, dual phosphorylated form of mitogen-activated protein kinase (ERK) with a specific monoclonal antibody. Detection of the active state of the *Drosophila* epidermal growth factor receptor (DER) pathway allowed the visualization of gradients and boundaries of receptor activation, assessment of the distribution of activating ligands, and analysis of interplay with the inhibitory ligand Argos. This in situ approach can be used to monitor other receptor-triggered pathways in a wide range of organisms.

Receptor-tyrosine kinases participate in diverse biological processes and trigger, by way of Ras, a sequential activation of protein kinases called the mitogen-activated protein (MAP) kinase signaling cascade (*1*). Several RTKs have been identified in *Drosophila*. Whereas some RTKs control a single developmental decision, DER functions in numerous developmental processes (*2–7*). Regulation of DER activation is often achieved by the restricted processing of an activating ligand, Spitz (*8*, *9*), and induction of the secreted inhibitory protein Argos (*10*).

MAP kinase (ERK) is activated by dual phosphorylation of threonine and tyrosine residues by MEK (*1*). A monoclonal antibody, termed diphospho-ERK (dp-ERK), was raised against a dually phosphorylated 11–amino acid peptide that constitutes the vertebrate ERK activation loop (*11–13*). All 11 residues are conserved in the single *Drosophila* ERK homolog Rolled (*14*), raising the possibility of cross-reactivity.

To study recognition specificity, we tested the antibody on *Drosophila* Schneider S2 cells expressing DER. Incubation with secreted Spitz (sSpitz) resulted in the detection of a single 44-kD polypeptide by dp-ERK antibody (Fig. 1A). A general polyclonal antibody to ERK detected a similarly sized polypeptide in the presence or absence of Spitz. Immunohistochemical staining of induced cells detected activated ERK (Fig. 1B) (*15*).

In embryos, activation of DER by ubiquitous sSpitz (HS-sSpi) resulted in the accumulation of a single 44-kD polypeptide detected by dp-ERK antibody (Fig. 1A). Immunohistochemical staining of embryos with the general antibody to ERK displayed ubiquitous staining throughout embryogenesis in accordance with the high maternal contribution of the *rolled* gene. In contrast, dp-ERK displayed a specific staining pattern. Local activation of DER in the central segments led to staining only in this part of the embryo (Fig. 1C) (*16*).

Because ERK is a common junction for RTK pathways, the dp-ERK staining pattern represents the composite pattern of RTK signaling during development and can be correlated with activity of the known RTKs: Torso, DER, Heartless, and Breathless (*17*). Here we examine the dynamic DER-induced dp-ERK patterns in the embryo and imaginal discs.

Activation of DER is triggered by processing of Spitz, which is regulated by two membrane-spanning proteins, Rhomboid (Rho) and Star (*8*, *18*, *19*). Expression of Rho is tightly controlled (*18*, *20*), and its

L. Gabay and B.-Z. Shilo, Department of Molecular Genetics, Weizmann Institute of Science, Rehovot 76100, Israel.
R. Seger, Department of Membrane Research and Biophysics, Weizmann Institute of Science, Rehovot 76100, Israel.

*To whom correspondence should be addressed. E-mail: lvshilo@weizmann.weizmann.ac.il

ectopic induction leads to deregulated activation of DER (9, 21). It was not known whether the initial expression of Rho in the neuroectoderm before gastrulation leads to DER activation, because no phenotypes in *spitz*, *rho*, or *DER* mutants were assigned to this phase. dp-ERK distribution during the early stages of embryogenesis was identical to the Rho expression pattern. This early zygotic dp-ERK pattern was absent in embryos mutant for *spitz*, *rho*, or *DER* genes, demonstrating that it is generated by Spitz-induced DER activation (Fig. 2, A to C).

At stages 7 to 9, the dp-ERK pattern is driven by Rho expression in the cephalic furrow, three head furrows, and the two dorsal folds. This pattern was absent in *rho* or *DER* mutants (Fig. 2, D and E), although no defects in furrow formation were detected. Whereas localized DER activation could provide the spatial and temporal cue to initiate furrows, another pathway may function in parallel.

The earliest known zygotic function of DER in patterning the ventral ectoderm at stage 9/10 is induced by Spitz, which is processed in the midline cells (9) to produce an active ligand. The extent of sSpitz diffusion and the levels of DER activation induced in the different ectodermal cell rows were not known. A graded dp-ERK pattern was observed in three to four cell rows on each side of the ventral midline, with the strongest staining displayed by cells adjacent to the midline (Fig. 2, F and H). This ectodermal staining was absent in *spitz*, *rho*, or *DER* mutant embryos (Fig. 2G), as well as in *single minded* mutant embryos that lack a functional midline. Thus, the midline is the only source of ligand for the ventral ectoderm at stage 9/10.

An inhibitory ligand, Argos, modulates the pattern of DER activation. *argos* transcription is induced by the DER pathway, thus constituting a negative-feedback loop. *argos* expression in the ventral-most cells,

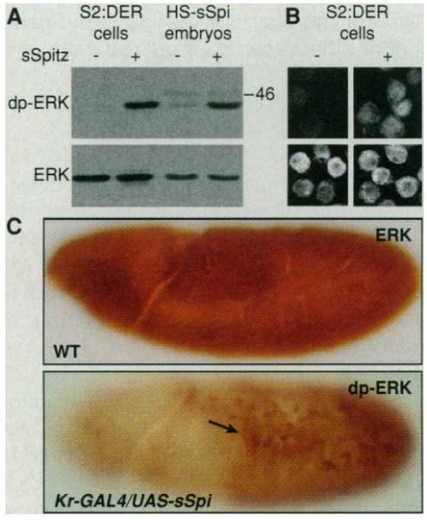

Fig. 1. Detection of dp-ERK in Schneider cells and embryos. (**A**) S2 cells expressing DER (S2:DER) were incubated with secreted Spitz (sSpitz). A 44-kD band was resolved by SDS-PAGE and detected with the anti–dp-ERK. The general antibody to ERK detected a similar molecular weight band with equal intensities before and after incubation with sSpitz. sSpitz was also induced in embryos containing *K25 HS-Gal4/UAS-secreted Spitz* (HS-sSpi). After heat shock, accumulation of the 44-kD band was detected by anti–dp-ERK, whereas the general antibody to ERK detected this band with or without sSpitz. (**B**) Immunohistochemical staining of S2 cells expressing DER showed accumulation of dp-ERK after incubation with sSpitz. (**C**) dp-ERK staining was monitored in *Kr-Gal4/UAS-secreted Spitz* embryos in which sSpitz was induced only in the central part of the embryo, and a uniform pattern was observed in this region (arrow shows anterior border of *Kr* domain; the posterior border is not seen in the image). Staining of a wild-type embryo at a similar stage (stage 11) with the general antibody to ERK showed a ubiquitous pattern throughout the embryo.

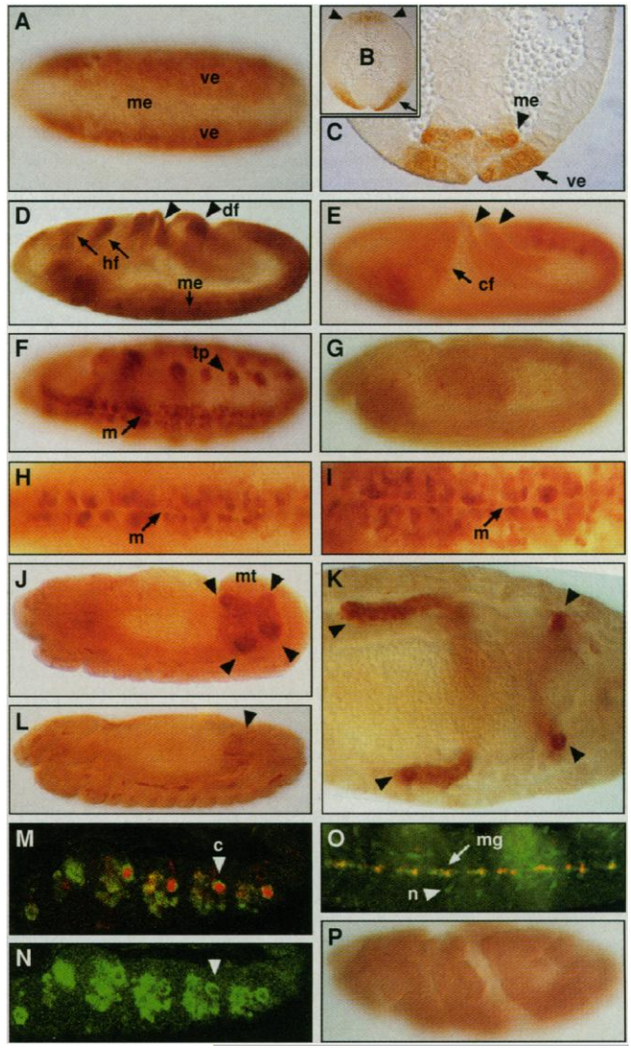

Fig. 2. DER-dependent ERK activation during embryogenesis. (**A**) At stage 7, dp-ERK was detected in the ventral ectoderm (ve) but not in the future mesoderm (me). (**B**) At stage 8 after mesoderm invagination, staining persists in the ventral ectoderm (arrow) and was also observed in the dorsal ectoderm (arrowheads). (**C**) Once the initial contact of the mesoderm with the ectoderm is established, dp-ERK was also detected in the mesodermal cells immediately adjacent to activated ectodermal cells. This is presumably induced by diffusion of sSpitz to the mesoderm. The staining in the ventral ectoderm declines by stage 9. (**D**) At stage 8 dp-ERK was monitored in the ventral ectoderm, the dorsal-anterior and dorsal-posterior folds (df), the cephalic furrow, the head folds (hf), and the mesoderm. (**E**) Except for the mesodermal staining, all of the above aspects are induced by DER, because these patterns were absent in $rho^{\Delta 38}$ null mutants. However, the dorsal furrows (arrowheads) and cephalic furrow (cf) invaginated normally. (**F**) At stage 10, two prominent DER-dependent dp-ERK patterns were observed: the tracheal placodes (tp) and ventral ectoderm on both sides of the ventral midline (m). (**G**) Both of these patterns were eliminated in a $spitz^{OE92}$ mutant embryo. (**H**) Higher magnification of a stage 10 embryo shows graded distribution of dp-ERK, in three to four cells on each side of the midline. (**I**) In $argos^{\Delta 7}$ mutant embryos, this activation pattern was expanded to four to five rows of cells. (**J**) At stage 12, dp-ERK was detected in the four malpighian tubules (mt) (arrowheads). (**K**) Malpighian tubule staining intensity appears uniform and persists until stage 15. (**L**) The early malpighian tubule staining is DER-dependent, because it was absent in spi^{OE92} mutants. (**M**) At stage 11, the founder cells of the chordotonal organs (c) can be detected in each segment by *rho-lacZ* expression (red). (**N**) Dp-ERK (green) is excluded from the founder cells and was observed in a ringlike structure surrounding them. (**O**) At stage 15, dp-ERK (green) was detected in the midline glial cells (mg) marked by the enhancer trap line *AA142* (red). Staining in unidentified neurons (n) was also observed. (**P**) No dp-ERK was observed in a csw^{LE120} mutant embryos lacking both maternal and zygotic components. Shown is a stage 10 embryo.

followed by diffusion, was postulated to terminate or reduce DER signaling in the ventrolateral cells (*10*). In *argos* mutant embryos an expanded pattern of dp-ERK was observed, with an intensity similar to that normally observed in the cells adjacent to the midline (Fig. 2I). This correlates with the expansion of ventral-most cell fates monitored in this mutant background (*10*). Thus, Spitz can diffuse up to five cell rows on each side of the midline.

At stage 11, DER-dependent dp-ERK staining was observed in the chordotonal organs. These stretch receptor organs in the peripheral nervous system are initially induced as clusters of three cells, with additional cells recruited by activation of the DER pathway (*18*, *22*). This dp-ERK pattern was absent in *rho* mutant embryos. Double staining with a *rho-lacZ* reporter demonstrated that dp-ERK was present in a ringlike structure surrounding the Rho-expressing cells (Fig. 2, M and N). This may be consistent with the production of sSpitz in the primary cluster in order to recruit additional cells through the DER pathway. It is not clear why the chordotonal cells that express Rho are refractory to ERK activation. DER-induced dp-ERK staining was also observed in the tracheal placodes and malpighian tubules (Fig. 2, F, J, and K). Finally, the DER pathway is essential for the development and viability of the midline glial cells (*23*). Prominent dp-ERK staining was observed at stage 15 in these cells (Fig. 2O).

The ability to directly monitor the pattern of dp-ERK in the different mutant backgrounds provides a rapid and powerful tool to place genes in the signaling cascade with respect to ERK. The *corkscrew* (*csw*) gene, encoding an SH2 (SRC homology 2)-containing tyrosine phosphatase (*24*), is a case in point. Although *csw* was originally identified by an embryonic phenotype resembling that of *torso*, subsequent work has suggested that it may also be required for signaling by other RTKs (*24*). By monitoring the dp-ERK pattern in embryos lacking both maternal and zygotic *csw*, we have shown that all aspects of dp-ERK staining are diminished (Fig. 2P). Thus, Corkscrew is required for signaling by all RTKs and converges into the signaling pathway upstream of ERK.

A dynamic dp-ERK pattern identified in imaginal discs can be correlated with known DER functions. In the third-instar wing imaginal disc, prominent dp-ERK staining was detected in the future vein regions expressing Rho (*25*), including veins L3, L4, and L5, and in a transverse band of cells that will give rise to the wing margin. dp-ERK staining was also observed in the notum, along the posterior margin, and in the anterior mesopleura (Fig. 3) (*26*).

The interplay between activating and inhibiting DER ligands was monitored during development of the eye imaginal disc. At the morphogenetic furrow, prominent dp-ERK staining was observed in the newly formed photoreceptor clusters. Staining was also detected in clusters posterior to the first row, but at a lower intensity (Fig. 4, A and C). During ommatidial differentiation, successive cycles of photoreceptor recruitment through the DER pathway take place. Activation of DER by sSpitz gives rise to the induction of Argos expression, preventing Spitz from activating DER in the more distal cells by a mechanism termed remote inhibition (*5*). When the production of sSpitz overcomes this inhibition, a new cycle of activation is initiated.

Only in the first photoreceptor row, sSpitz activates DER in the absence of Argos. Once *argos* is induced, its expression persists throughout all stages of photoreceptor, cone, and pigment cell differentiation (*10*). Double staining of dp-ERK and Argos showed that Argos is present only in the region with weak dp-ERK staining (Fig. 4D). The causal role of Argos in reducing the dp-ERK intensity was demonstrated in eye discs homozygous for the hypomorphic *argos*^{W11} mutation. In this case, the posterior rows also showed strong dp-ERK staining (Fig. 4B).

In addition to the reduction in dp-ERK intensity posteriorly, a parallel alteration in its spatial distribution within each ommatidial cluster was observed. Only one to three centrally located cells were labeled in each cluster in the anterior row. As ommatidia matured, staining diminished in the central cells and was observed in the periphery of each cluster (Fig. 4, E and F). The postulated reiterative cycles of DER activation in the

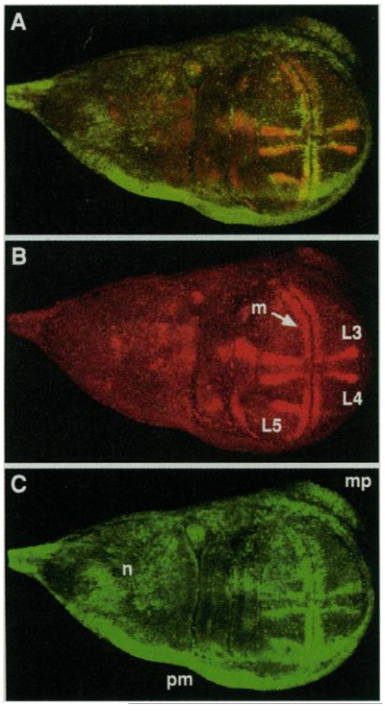

Fig. 3. Dp-ERK in the wing imaginal disc. Third instar wing imaginal disc from larvae heterozygous for an *argos*$^{l(3)5959}$ enhancer trap, stained with anti–β-Gal (red) and dp-ERK (green). (**A**) Composite image. (**B**) Position of wing vein primordia (L) and wing margin (m) are marked. (**C**) In addition to prominent dp-ERK staining in the vein primordia, staining was also detected at several sites of Vein expression including the notum (n), lateral anterior mesopleura (mp), and posterior margin (pm). Vein is a putative DER ligand (*27*). No dp-ERK was detected in the inter-vein 3-4 region, which is also a prominent site of Vein expression. Anterior is at the top.

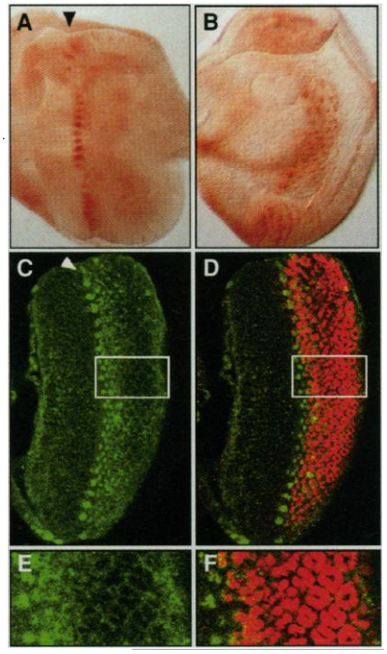

Fig. 4. Dp-ERK in the eye imaginal disc. (**A**) Third-instar eye imaginal disc showed the most prominent dp-ERK staining in the row of photoreceptor clusters immediately posterior to the morphogenetic furrow (arrowhead). More posterior ommatidial rows showed less staining. (**B**) In discs derived from larvae homozygous for the hypomorphic *argos*^{W11} mutation, the intensity of dp-ERK in the posterior rows was comparable to that of the most anterior one. (**C**) Eye disc derived from a heterozygous *argos*$^{l(3)5959}$ enhancer trap line. Dp-ERK (green) is most prominent at the first row. (**D**) Argos expression (red) was observed after the first row and may thus account for the lower dp-ERK intensity in all posterior rows. (**E** and **F**) Enlargements showing that at the time of formation of the ommatidia, dp-ERK staining is strong and centrally located. As differentiation proceeds, the more posterior ommatidia show exclusion of dp-ERK from the central cells expressing *argos* and activation in a ring around each ommatidium. The rings expand as the ommatidia mature. Anterior is to the left.

eye disc (5) may thus be visualized as expanding concentric rings of dp-ERK.

In accordance with the multiple functions of DER during development, many of the dp-ERK patterns are attributed to DER activation. The temporal and spatial correlation of DER-induced dp-ERK to Rho expression stands out. The only exception is the activation of DER in the ventral ectoderm at stage 10 that is induced by Spitz-processing machinery restricted to the midline. These findings point to Rho as the limiting element in activation of the DER pathway. Different ranges of diffusion were observed for Spitz in different biological contexts, highlighting the importance of molecules that may restrict or facilitate ligand diffusion in regulating the spatial pattern of receptor activation.

REFERENCES AND NOTES

1. R. Seger and E. G. Krebs, *FASEB J.* **9**, 726 (1995).
2. R. Schweitzer and B.-Z. Shilo, *Trends Genet.* **13**, 191 (1997).
3. E. Raz and B. Z. Shilo, *Genes Dev.* **7**, 1937 (1993).
4. F. J. Diaz-Benjumea and A. Garcia-Bellido, *Proc. R. Soc. London Ser. B* **242**, 36 (1990).
5. M. Freeman, *Cell* **87**, 651 (1996).
6. M. Tio and K. Moses, *Development* **124**, 343 (1997).
7. T. Schüpbach, *Cell* **49**, 699 (1987); A. González-Reyes, H. Elliot, D. St. Johnston, *Nature* **375**, 654 (1995); S. Roth, F. S. Neuman-Silberberg, G. Barcelo, T. Schüpbach, *Cell* **81**, 967 (1995).
8. R. Schweitzer, M. Shaharabany, R. Seger, B.-Z. Shilo, *Genes Dev.* **9**, 1518 (1995).
9. M. Golembo, E. Raz, B.-Z. Shilo, *Development* **122**, 3363 (1996).
10. M. Freeman, C. Klämbt, C. S. Goodman, G. M. Rubin, *Cell* **69**, 963 (1992); R. Schweitzer, R. Howes, R. Smith, B.-Z. Shilo, M. Freeman, *Nature* **376**, 699 (1995); M. Golembo, R. Schweitzer, M. Freeman, B.-Z. Shilo, *Development* **122**, 223 (1996).
11. The activated monoclonal antibody to MAPK (dp-ERK) was raised against the 11–amino acid peptide His-Thr-Gly-Phe-Leu-Thr-(P_t)-Glu-Tyr-(P_t)-Val-Ala-Thr corresponding to the phosphorylated form of the ERK-activation loop.
12. The general rabbit polyclonal antibody to ERK (Ab. 7884) was generated against a 23–amino acid peptide from subdomain XI [K. C. Gause *et al.*, *J. Biol. Chem.* **268**, 16124 (1993)].
13. Y. Yung *et al.*, *FEBS Lett.* **408**, 292 (1997).
14. W. Biggs and S. L. Zipursky, *Proc. Natl. Acad. Sci. U.S.A.* **89**, 6295 (1992).
15. D2f (8) or Schneider cells were incubated with medium containing sSpitz for 12 min. After incubation the cells were lysed with sample buffer, and lysates were separated on a 12% SDS–polyacrylamide gel electrophoresis (PAGE) gel. After blotting to nitrocellulose, the general antibody to ERK was detected with a 1/10,000 dilution of Ab. 7884, and dp-ERK was detected with a 1/2000 dilution of anti–dp-ERK. For induction of dp-ERK in embryos, embryos containing *sev-hs-Gal4* and *UAS-secreted Spitz4a* were collected for 5 hours, administered heat shock at 37°C for 20 min, incubated at 29°C for 1 hour, and lysed. Control embryos of the same genotype were treated identically, but heat shock was eliminated.
16. Cells were fixed in 4% formaldehyde (fresh) for 20 min. After washes, the cells were permeabilized with 0.5% Triton X-100 in phosphate-buffered saline for 5 min. Subsequent steps were standard. Fresh embryos were fixed in 8% formaldehyde and kept in 100% methanol at −20°C. All washes were done with PBS, 0.1% Tween-20. In cases of DAB or fluorescent double stainings, the second primary antibody was added only after completion of washes of the secondary antibody to dp-ERK to ensure efficient staining and avoid cross-reactivity. All other aspects of staining were standard. After preincubation of anti–dp-ERK with the phosphorylated peptide antigen, staining was eliminated. Other antibodies used include rabbit anti–β-Gal (Cappel). Secondary antibodies include horseradish peroxidase–conjugated goat anti-mouse immunoglobulin G (IgG) and fluorescein isothiocyanate– or LRSC-conjugated goat anti-mouse IgG+IgM or anti-rabbit IgG (Jackson labs).
17. L. Gabay, R. Seger, B.-Z. Shilo, *Development* **124**, 3535 (1997).
18. E. Bier *et al.*, *Genes Dev.* **4**, 190 (1990).
19. A. L. Kolodkin, A. T. Pickup, D. M. Lin, C. S. Goodman, U. Banerjee, *Development* **120**, 1731 (1994).
20. Y. T. Ip, R. E. Park, D. Kosman, E. Bier, M. Levine, *Genes Dev.* **6**, 1728 (1992).
21. R. Noll, M. A. Sturtevant, R. R. Gollapudi, E. Bier, *Development* **120**, 2329 (1994); H. Xiao, L. A. Hrdlicka, J. Nambu, *Mech. Dev.* **58**, 65 (1996).
22. B. J. Rutledge, K. Zhang, E. Bier, Y. N. Jan, N. Perrimon, *Genes Dev.* **6**, 1503 (1992); P. zur Lage, Y. N. Jan, A. P. Jarman, *Curr. Biol.* **7**, 166 (1997); M. Okabe and H. Okano, *Development* **124**, 1045 (1997).
23. C. Klämbt, J. R. Jacobs, C. S. Goodman, *Cell* **64**, 801 (1991); E. Raz and B.-Z. Shilo, *Development* **114**, 113 (1992); H. Scholz, E. Sadlowski, A. Klaes, C. Klämbt, *Mech. Dev.* **62**, 79 (1997).
24. L. A. Perkins, I. Larsen, N. Perrimon, *Cell* **70**, 225 (1992); L. A. Perkins, M. R. Johnson, M. B. Melnik, N. Perrimon, *Dev. Biol.* **180**, 63 (1996).
25. M. A. Sturtevant *et al.*, *Genes Dev.* **7**, 961 (1993).
26. Fixation of imaginal discs was carried out in 4% formaldehyde for 30 min. Wash solutions contained 0.2% Triton X-100. In contrast to anti–dp-ERK staining of embryos, which is highly reproducible, staining of imaginal discs is variable, for unknown reasons.
27. B. Schnepp, G. Grumbling, T. Donaldson, A. Simcox, *Genes Dev.* **10**, 2302 (1996); A. A. Simcox *et al.*, *Dev. Biol.* **177**, 475 (1996).

28. We thank Y. Dolginov and D. Zharhary (Sigma Israel Chemicals, Rehovot, Israel) for help preparing activated antibody to MAPK (dp-ERK), and A. Brand, S. Crews, M. Freeman, W. Gehring, E. Hafen, C. Klämbt, M. Leptin, M. Levine, L. Perkins, and N. Perrimon for providing antibodies and fly stocks. We thank members of the Shilo lab, R. Schweitzer, and T. Volk for critical reading of the manuscript. R.S. is an incumbent of the Samuel and Isabela Friedman Career Development Chair. Supported by a grant from the Dr. Josef Cohn Minerva Center for Biomembrane Research (R.S.) and by grants from the Tobacco Research Council, US-Israel binational fund, UK-Israel binational fund, and Minerva Foundation (B.-Z.S.).

25 March 1997; accepted 7 July 1997

Thermophilic Fe(III)-Reducing Bacteria from the Deep Subsurface: The Evolutionary Implications

Shi V. Liu,* Jizhong Zhou, Chuanlun Zhang, David R. Cole, M. Gajdarziska-Josifovska, Tommy J. Phelps†

Thermophilic (45° to 75°C) bacteria that reduce amorphous Fe(III)-oxyhydroxide to magnetic iron oxides have been discovered in two geologically and hydrologically isolated Cretaceous- and Triassic-age sedimentary basins in the deep (>860 meters below land surface) terrestrial subsurface. Molecular analyses based on 16S ribosomal RNA (rRNA) gene sequences revealed that some of these bacteria represent an unrecognized phylogenetic group of dissimilatory Fe(III)-reducing bacteria. This discovery adds another dimension to the study of microbial Fe(III) reduction and biogenic magnetism. It also provides examples for understanding the history of Fe(III)-reducing microorganisms and for assessing possible roles of such microorganisms on hot primitive planets.

Dissimilatory Fe(III) reduction is proposed to be an early form of microbial respiration (*1*), and it may have influenced the geochemistry and the paleomagnetism of the Archaean Earth (*2*). Microbial Fe(III) reduction has been observed primarily in low-temperature environments that have been extensively influenced by modern surface processes (*3*). Previous studies on dissimilatory Fe(III)-reducing bacteria have been focused on mesophilic microorganisms within *Proteobacteria* (*4*), which are located distant from the deep branches on the phylogenetic tree (*5*). The paucity of information on thermophilic dissimilatory Fe(III)-reducing microorganisms (*6*) is striking in that thermophilic species are frequently found in many other groups of microorganisms such as methanogens, sulfate-reducing bacteria, and acetogens (*7*). This lack of information presents a difficulty in explaining microbial Fe(III) reduction on primitive Earth, which was reputedly warmer than Earth is now (*8*). Although the geological evidence for microbial Fe(III) reduction in Archaean Earth is recognized (*2*), the early evolution of microbial Fe(III)-reducing microorganisms on Earth has not yet been de-

S. V. Liu, J. Zhou, C. Zhang, T. J. Phelps. Environmental Sciences Division, Oak Ridge National Laboratory, Post Office Box 2008, Oak Ridge, TN 37831–6036, USA.
D. R. Cole. Chemical and Analytical Sciences Division, Oak Ridge National Laboratory, Post Office Box 2008, Oak Ridge, TN 37831–6110, USA.
M. Gajdarziska-Josifovska, Department of Physics, University of Wisconsin, Post Office Box 413, Milwaukee, WI 53201, USA.

*Present address: Department of Microbiology and Immunology, Allegheny University of the Health Sciences, Philadelphia, PA 19129, USA.
†To whom correspondence should be addressed.